VIP Helicenes Very Important Paper

How to cite:
International Edition: doi.org/10.1002/anie.202012213
German Edition: doi.org/10.1002/ange.202012213

Elucidation of Diverse Solid-State Packing in a Family of Electron-Deficient Expanded Helicenes via Microcrystal Electron Diffraction (MicroED)**

Adrian E. Samkian[+], Gavin R. Kiel[+], Christopher G. Jones, Harrison M. Bergman, Julia Oktawiec, Hosea M. Nelson, and T. Don Tilley**

Abstract: *Solid-state packing plays a defining role in the properties of a molecular organic material, but it is difficult to elucidate in the absence of single crystals that are suitable for X-ray diffraction. Herein, we demonstrate the coupling of divergent synthesis with microcrystal electron diffraction (MicroED) for rapid assessment of solid-state packing motifs, using a class of chiral nanocarbons—expanded helicenes—as a proof of concept. Two highly selective oxidative dearomatizations of a readily accessible helicene provided a divergent route to four electron-deficient analogues containing quinone or quinoxaline units. Crystallization efforts consistently yielded microcrystals that were unsuitable for single-crystal X-ray diffraction, but ideal for MicroED. This technique facilitated the elucidation of solid-state structures of all five compounds with <1.1 Å resolution. The otherwise-inaccessible data revealed a range of notable packing behaviors, including four different space groups, homochirality in a crystal for a helicene with an extremely low enantiomerization barrier, and nanometer scale cavities.*

Introduction

There is growing interest in chirality as an orthogonal design element for next-generation molecular organic materials.[1] This parameter gives rise to new properties as a result of its impact on electronic structure, including circularly polarized absorption and emission,[2] nonlinear optical behavior,[3] and spin polarization.[4] While the impact of chirality on *molecular* properties is important, its impact on *supramolecular and solid-state* behavior is especially relevant if the molecule is to be integrated into a material or device.[5] The low symmetry and diverse geometries of chiral molecules have profound implications for the properties of their aggregates, but the complexities of such structures severely complicate efforts toward rational design.[6]

As the prototypical chiral aromatic molecules, helicenes—helical arrays of fused aromatic rings—have been at the forefront of efforts to exploit chirality in organic (opto)electronic applications.[1d-f] The structural diversity of these compounds has recently grown at a rapid rate, with a particular surge of structures containing multiple helicenes embedded into larger polyaromatic frameworks.[7] Helicenes exhibit remarkable supramolecular and solid-state chemistry promoted by π-stacking interactions, which can result in enhanced or emergent properties.[3,7c,8] For example, using a versatile helicene quinone scaffold, Nuckolls, Katz, and Verbiest demonstrated significant enhancements of specific rotation, circular dichroism, and second-order nonlinear optical susceptibility due to aggregation.[3,8a] More recently, Itami and co-workers reported a double helicene that exhibits π-stacking in all three crystallographic dimensions, a rare phenomenon that may give rise to isotropic charge transport.[7c] Along these lines, the unique solid-state behavior of helicenes has been exploited in a device setting. For example, in an organic field effect transistor, the enantiopurity of the helicene-based active layer can have dramatic or unexpected effects on performance.[2b,8b–d] Nakamura demonstrated that a charge carrier inversion (switch from p- to n-type) can occur on going from a racemic to an enantiopure helicene[8b] and Fuchter observed an 80-fold increase in charge carrier mobility for a racemic active layer (vs. an enantiopure analogue).[8c] These results motivate further research related to helicene solid-state structure and highlight the important role of chirality.

In 2017, the Tilley group introduced a new class of chiral nanocarbons, "expanded helicenes," which possess internal cavities and large diameters due to alternating angular and linear ring fusion (e.g. **1a**,**b**, Scheme 1a).[9] One exciting feature of these compounds is their unique self-assembly and solid-state packing, facilitated in part by their structural flexibility. For example, expanded [13]helicene **1b** dimerizes via π-stacking to form the unusual double helix **1b-Dim**, both in chloroform-*d* solution and in the solid-state, which is accompanied by a large (>2×) increase in the pitch of the constituent helicenes.[9a] In contrast, no aggregation was apparent for the [11]helicene analogue (**1a**). Subsequently, the covalent linkage of two expanded helicenes afforded a configurationally labile "Figure-eight" dimer that crystal-

[*] A. E. Samkian,[+] G. R. Kiel,[+] H. M. Bergman, J. Oktawiec, T. D. Tilley
Department of Chemistry, University of California, Berkeley
Berkeley, CA 94720 (USA)
E-mail: tdtilley@berkeley.edu
C. G. Jones, H. M. Nelson
Department of Chemistry and Biochemistry, University of California, Los Angeles
Los Angeles, CA 90095 (USA)
E-mail: hosea@chem.ucla.edu
[+] These authors contributed equally to this work.

[**] A previous version of this manuscript has been deposited on a preprint server (https://doi.org/10.26434/chemrxiv.12925511.v2).
Supporting information and the ORCID identification number(s) for the author(s) of this article can be found under: https://doi.org/10.1002/anie.202012213.

lized into an intricate homochiral network containing two distinct yet interconnected helical superstructures.[9c]

Single crystal X-ray diffraction is the gold standard for solid-state structure elucidation since it can provide structural parameters with a high level of precision; however, even for crystalline compounds, it can be difficult or impossible to obtain suitable single crystals for analysis, which can preclude valuable insights. For example, our inability to obtain suitable crystals of **1a** prevented comparisons with its apparently more interesting analogue **1b**.[9a] Microcrystal electron diffraction (MicroED) has recently emerged as a way to circumvent limitations related to crystal growth since it can allow high-resolution structural data to be acquired on *nano*crystalline samples.[10]

In this contribution, we use a combination of divergent synthesis and MicroED to interrogate solid-state behavior in a new family of expanded helicenes. The quinone- and quinoxiline-containing helicenes **2-mon**, **2-di**, **3-mon**, and **3-di** (Scheme 1b) were targeted due to their electron deficiency, which tends to promote strong intermolecular interactions between π-systems.[8a,11] The new compounds were accessed via a highly selective oxidative dearomatization of electron-rich **1a**, which provided derivatives of the same or reduced symmetry. While uncontrollable crystallization kinetics consistently resulted in the formation of microcrystals that were unsuitable for single crystal X-ray diffraction, the application of MicroED enabled the rapid acquisition of high resolution data for all five helicenes. This data revealed three different packing motifs, representing four different space groups.

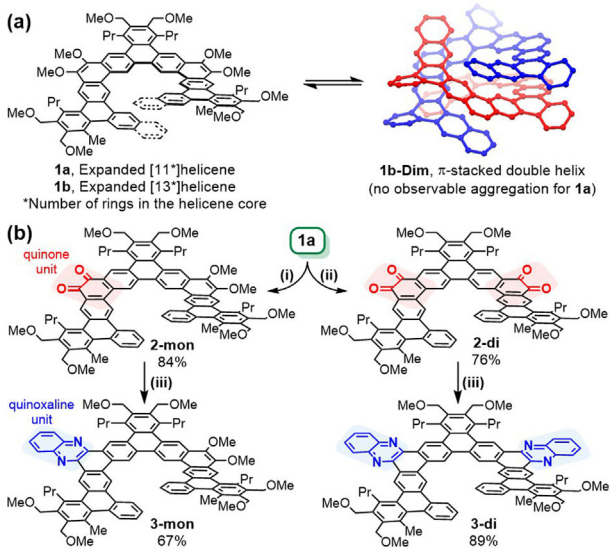

Scheme 1. a) Previous Work: Expanded [11]- and [13]helicenes **1a** and **1b**, and the observation of π-stacked double helix **1b-Dim** (both in solution and the solid-state). Compound **1a** could not be analyzed by X-ray crystallography owing to the difficulty in obtaining suitable single crystals; b) This work: A simple post-synthetic oxidation of electron-rich and non-aggregating **1a** provided rapid, divergent access to electron-deficient analogues **2-di** and **3-di** and donor–acceptor analogues **2-mon** and **3-mon**. Conditions: i) CAN (6 equiv), CH_2Cl_2, MeCN, H_2O, 22 °C; ii) CAN (15 equiv), CH_2Cl_2, MeCN, H_2O, 22 °C; iii) 1,2-diaminobenzene (5 and 20 equiv for **3-mon** and **3-di**, respectively), DCE, 70 °C.

Three of the structures feature large (1.3–2.0 nm) channels, enforced by the ability of the helicenes to accommodate large distortions in molecular geometry.

Results and Discussion

Quinone-containing helicenes display desirable properties due to their low LUMO levels, including red-shifted absorption, reversible redox behavior, and strong aggregation.[8a,12] Furthermore, polycyclic aromatic hydrocarbons (PAHs) with quinone functionalities are well-established synthons for a range of derivatives, including π-extended cyclopentadienones,[13] imidazoles,[14] and pyrazines,[15] which facilitates divergent manipulation of properties.[16] An expedient way to install quinone units is via the oxidation of a PAH with a 1,2-dimethoxy substitution pattern.[16a,17] Since compound **1a** is available using a scalable procedure,[9a] this strategy seemed to represent an opportunity to significantly increase functional diversity in expanded helicenes. Thus, in an attempt to fully oxidize **1a** to its diquinone derivative **2-di** (Scheme 1b), this compound was treated with an excess (6 equiv) of cerium ammonium nitrate (CAN) in a CH_2Cl_2/MeCN/H_2O solvent system. Remarkably, this instead resulted in the selective formation of monoquinone **2-mon**, isolated in 84% yield. The exceptional selectivity for **2-mon** over **2-di** is surprising given the highly benzenoid nature of **1a** and its quinone derivatives, which is expected to limit electronic communication across the π-system.[18] This suggests that inductive effects play an important role in slowing down the oxidation of the second 1,2-dimethoxyarene unit even though the two reaction sites are physically distant. Importantly, diquinone **2-di** was also accessed, in 76% yield, simply with use of a larger excess of CAN (15 equiv).

The condensation of a 1,2-diamine onto a quinone-containing PAH is a reliable and general transformation that provides a means to install functionally-valuable nitrogen atoms and extend the π-system,[15] which could lead to stronger π-stacking interactions between molecules.[11] Thus, **2-mon** and **2-di** were treated with excess 1,2-phenylenediamine in 1,2-dichloroethane (DCE) at 70 °C, which afforded quinoxaline-containing helicenes **3-mon** and **3-di** in 67% and 89% isolated yields, respectively, after a simple workup/purification procedure consisting of precipitation followed by recrystallization from toluene. The identities of all new helicenes were initially confirmed with ^1H and ^{13}C NMR spectroscopies and high-resolution mass spectrometry (HRMS-ESI). Furthermore, the structures for all five helicenes were unambiguously confirmed by MicroED (see below).

The substitution of PAHs with quinone units often results in solubility problems,[17b,19] but the new helicenes **2-mon** and **2-di** are highly soluble (> 100 mg mL^{-1} in $CHCl_3$ and CH_2Cl_2). This is especially notable given their large size (14 fused rings). The solubility may be attributed to two different forms of non-planarity: 1) the helical distortion that is present in all helicenes and 2) a bending of the benzannulated rings away from the contour of the helix, which results from alkyl substituents in six different bay positions. While the quinoxa-

line-annulated helicenes **3-mon** and **3-di** are similarly soluble to the quinone analogs in a thermodynamic sense, their kinetic solubility is low when isolated as a crystalline solid.

The photophysical properties of the new helicenes were probed by UV/Vis absorption and emission spectroscopies (Figure 1 a,b). Most notable are the sizable decreases in photophysical HOMO–LUMO gaps (calculated from their absorption onset values) for quinone-containing helicenes **2-mon** (2.08 eV) and **2-di** (2.05 eV) relative to that for their synthetic precursor **1a** (2.79 eV). In contrast, the quinoxaline units have only a small effect on this value (2.63 eV for both **3-mon** and **3-di**). Relative to the absorption maxima for **1a** (324 nm), small red shifts of 9 and 15 nm are observed for the mono- and diquinones **2-mon** and **2-di**, respectively, whereas blue shifts of comparable magnitude (5 and 9 nm) are observed for the mono- and diquinoxalines **3-mon** and **3-di**. Despite limited perturbation of their absorption maxima and onset values, **3-mon** and **3-di** display relatively large bathochromic shifts in emission maxima relative to that for **1a** (from 446 nm to 533 and 517 nm, respectively). As is typical for PAHs containing quinone units,[20] **2-mon** and **2-di** are non-emissive.

The electrochemical behavior of the helicenes was investigated by cyclic voltammetry (CV) in CH_2Cl_2 solution (Figure 1 c). Only **1a**, **2-mon**, and **3-mon** display oxidation events (one per 1,2-dimethoxy substituent), which were quasi-reversible or irreversible. The four new compounds with quinone or quinoxaline units display one reversible reduction event per unit (e.g. the presence of two quinones in **2-di** gives rise to two reversible reduction events).[21] The electrochemical HOMO–LUMO gaps for **2-mon** and **3-mon** (1.94 and 2.57 eV, respectively) are slightly smaller than those calculated from the absorption onset (see above). Replacement of the 1,2-dimethoxyarene units with quinone or quinoxaline units does not significantly affect HOMO energy levels. Compared to the HOMO level for **1a** (−5.46 eV), only slight decreases were observed for each additional quinone

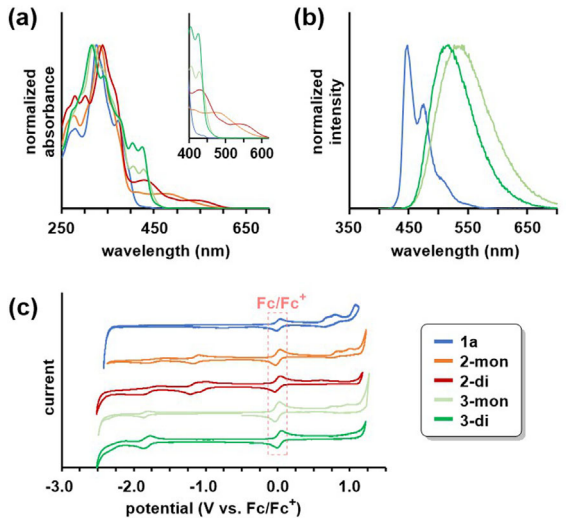

Figure 1. UV/Vis a) absorption and b) emission spectra in CH_2Cl_2; c) Cyclic voltammograms in CH_2Cl_2 (1.0 mM) with 0.1 M $^nBu_4NPF_6$ as the supporting electrolyte, scanned at 100 mV s^{-1}.

(≈0.15 eV) or quinoxaline (≈0.06 eV) unit. The large changes in HOMO/LUMO gaps result primarily from changes in LUMO levels (≈1.0 eV decreases for **2-mon** and **2-di** and ≈0.3 eV decreases for **3-mon** and **3-di**).

One of the primary motivations for structural modifications of compound **1a** was its limited aggregation via π-stacking. Aggregation behavior was initially probed by variable concentration ^{1}H NMR spectroscopy in chloroform-*d* solution. Like its precursor **1a**, monoquinone **2-mon** does not appear to aggregate to an appreciable extent in this solvent, as evidenced by the invariance of its ^{1}H NMR spectrum to concentration (Figures S9 and S10). In contrast, the ^{1}H NMR spectra of **2-di**, **3-mon**, and **3-di** all exhibit concentration dependence (Figures S11-S13). The most dramatic effects are observed for **3-di**, whose chemical shifts are shielded by up to 1.3 ppm upon concentration from 0.024 mM to 80 mM. In contrast, the chemical shifts of monoquinoxaline **3-mon** and diquinone **2-di** exhibit a combination of shielding and de-shielding, and of a smaller magnitude. Compounds **2-di**, **3-mon**, and **3-di** are rare in that they simultaneously aggregate and exhibit high solubility, without the need for long alkyl chains on the periphery. Since these two properties are usually at odds with one another, and since both are of critical importance for applications (e.g. in organic electronics), further elucidation of the nature of the aggregation was of interest.

Dynamic light scattering (DLS) experiments were conducted to probe aggregate size in chloroform solution (Figure S24). Measurements were made for diquinone **2-di** and diquinoxaline **3-di** since their variable concentration ^{1}H NMR spectra suggest notable aggregation, and the non-aggregating parent helicene **1a** was analyzed for comparison. As expected, the DLS measurements suggest that **1a** is monomeric regardless of concentration, at an average size of ≈1.0 nm.[22] In contrast, the size of **2-di** exhibits strong concentration dependence, from 1.0 nm at 0.24 mM (consistent with monomeric **2-di**) to 271 nm at 24 mM (consistent with supramolecular polymers). For diquinoxaline **3-di**, the size approaches 1.7 nm at high concentration, which suggests that the large upfield shifts observed in the ^{1}H NMR spectra of concentrated solutions result from small aggregates.

The observation of small aggregates for **3-di** via DLS prompted the use of the Horman/Dreux model for quantitative assessment of dimeric aggregation equilibria.[23] Using the aromatic chemical shifts from the variable concentration ^{1}H NMR spectra, this model provided an excellent fit and an average association constant for dimerization (K_a) of 13 M^{-1} at 298 K. Thus, these data are consistent with those from DLS, suggesting that higher-order aggregates of **3-di** do not play a significant role in the concentration range studied. The K_a value is slightly lower than that for expanded [13]helicene **1b** (23 M^{-1}),[9a] but these values may not be directly comparable since **1b** forms well-defined dimers (**1b-Dim**), whereas **3-di** may form aggregates with different molecularity.

Previously obtained crystal structures of expanded helicenes have revealed unique packing architectures and provided insight into their supramolecular interactions.[9] In pursuit of this information, significant effort was devoted to growing single crystals suitable for X-ray diffraction, but these

efforts consistently provided microcrystals[24] that were unsuitable (even with the aid of synchrotron radiation) for all compounds except **3-mon**. Thus, we turned to MicroED, and with this technique the structures of all five helicenes were elucidated with ease (Figure 2). The crystals used for analysis were grown as follows. For **1a**, the bulk, microcrystalline material obtained during its synthesis proved to be of sufficient quality. For **2-mon** and **2-di**, diffusion of pentane into an EtOAc solution yielded orange needles. For **3-mon** and **3-di**, slow evaporation of a benzene solution provided yellow rods.

The parent, electron-rich helicene **1a** crystallized in the chiral $P2_12_12_1$ space group, wherein the constituent molecules are homochiral and form weakly bound columns (Figure 2a). This is the second example of a homochiral expanded helicene crystal structure,[9c] and it is notable since **1a** is expected to have an extremely low enantiomerization barrier in solution.[9a-c] The closest π-stacking distance is 3.8 Å, and there are only two overlapping rings. These weak interactions are consistent with the absence of observable aggregation in chloroform-*d* solution.[9a] Notably, the packing is quite different than that of the isolated double helical dimers observed in the longer analogue **1b** (Figure 1a), which differs by only two rings at the terminus.

While the quinone-containing helicenes **2-di** and **2-mon** differ from **1a** only with respect to their oxidation state and associated methyl groups, all three compounds exhibit unique crystal packing. Compounds **2-di** and **2-mon** crystallized in the $P\bar{1}$ and *Iba*2 space groups, respectively (Figures 2b and 2c). In contrast to that of **1a**, these space groups are achiral. All three crystal structures feature columns driven by long-range π-stacking; however, in contrast to **1a** and **2-mon**, the columns of **2-di** are heterochiral (i.e. the helicenes within a given column alternate handedness), which leads to an achiral crystal. Individual columns for **2-mon** are homochiral, with alternation of chiralities between columns to make the overall structure achiral.

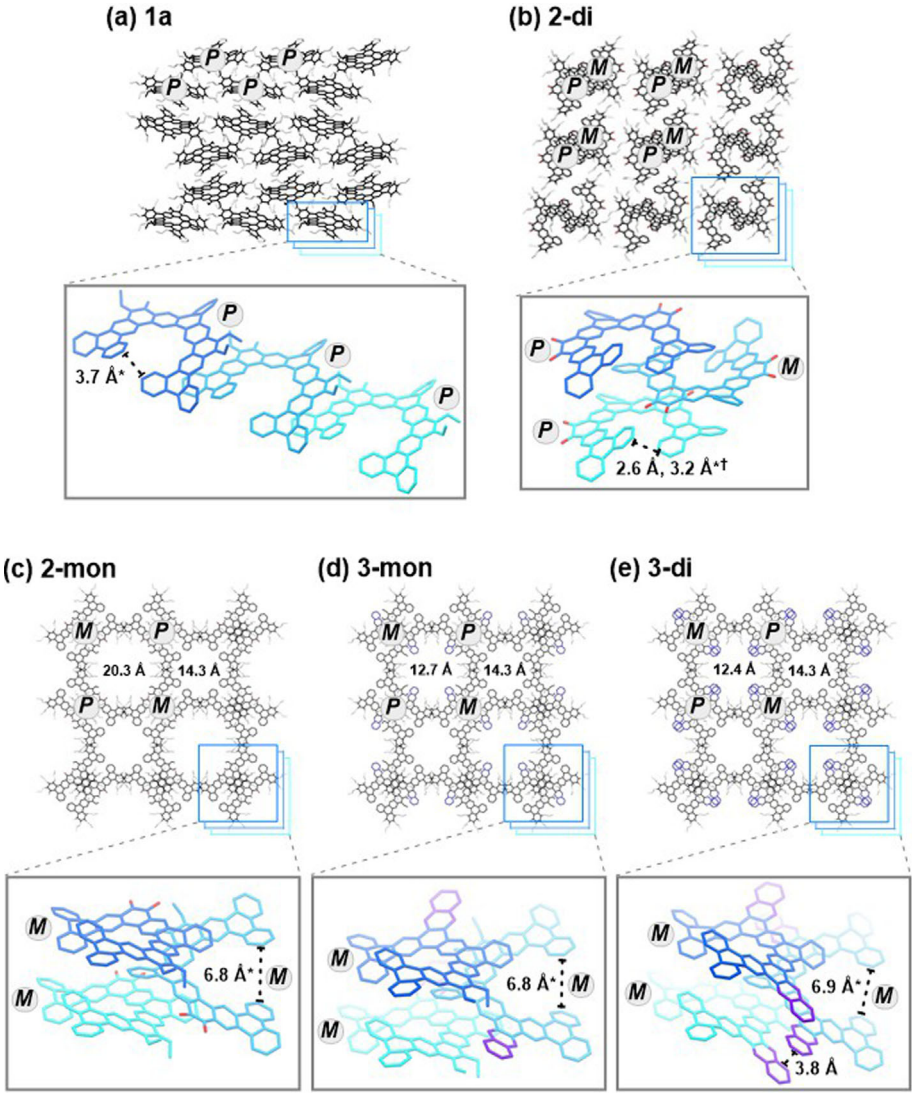

Figure 2. Solid-state MicroED structures of a) **1a**, b) **2-di**, c) **2-mon**, d) **3-mon**, and e) **3-di**. *The starred distances represent helical pitch values for the associated helicene, which were estimated as described in Figure 3. †The crystals of **2-di** feature helicenes with two different pitch values.

Compared to **1a**, the molecules of both quinone-containing helicenes exhibit more pronounced intermolecular interactions. This is especially true for **2-di**, which features eight overlapping rings per helicene and a closest π-contact of 3.4 Å. This close-packing appears to be driven by interactions between electron-deficient quinone units and relatively electron-rich benzannulated rings (two per molecule). The intermolecular interactions in **2-mon** support a complex framework with emergent macroscopic features, including the existence of two large cavities.

The crystal packings of **3-mon** and **3-di** (Figure 2d and e, respectively) are similar to that for **2-mon** in that all three exhibit a combination of one intrinsic and two extrinsic cavities. The intrinsic cavity ($\approx$4 Å in diameter) is consistent across all compounds since it is enforced by the alternating linear and angular ring fusion pattern that defines expanded helicenes. In all three cases, such cavities are occupied by the central methoxymethyl sidechains of neighboring molecules. There are two extrinsic cavities that emerge in each structure due to the packing arrangement. One is bordered by the terminal rings of the helicenes and is identical in all three structures (14.3 Å in diameter). The other differs for each helicene, and its size is dictated by the peripheral functionality (20.3 Å for **2-mon**, 12.7 Å for **3-mon**, 12.4 Å for **3-di**). While further examination of these cavities through the Fourier difference map shows some residual density, there is likely substantial disordered solvent present as this is generally accepted for a wide range of porous and macromolecular structures.[25] Like **2-mon**, compound **3-mon** also crystallized in the *Iba*2 space group, but compound **3-di** occupies the higher symmetry $I\bar{4}c2$ space group since it has a molecular C_2 axis. Each of these three helicenes has only one overlapping backbone ring with similar centroid-centroid distances (4.2 Å for **3-mon**, 4.0 Å for **3-di**, and 4.1 Å for **2-mon**) indicating weak interactions. In addition, **3-di** has overlapping quinoxaline units that may contribute to its strong aggregation in solution.

A striking feature of the MicroED structures is the large helical pitches for **2-mon**, **3-mon**, and **3-di** (6.8, 6.8, and 6.9 Å, respectively).[26] Previously reported expanded helicenes, and compounds **1a** and **2-di** described herein, have pitches in the range of 2.6–3.7 Å.[9] One exception is dimeric [13]helicene **1b-Dim** (Figure 1a),[9a] wherein each helicene displays a large pitch (7.4 Å) to accommodate extensive π-stacking. Another case where a notable molecular distortion was observed in the crystal structure was for the recently-reported Figure-eight expanded helicene dimer.[9c] There, an intricate network of π-stacking interactions appears to be the driving force for the distortion. In contrast to that for **1b-Dim** and the Figure-eight helicene, the driving forces for the observed, large molecular distortions are unclear.

The distorted molecular structures of **2-mon**, **3-mon**, and **3-di** in the solid-state suggest a high level of structural flexibility for these compounds, especially given the absence of notable intermolecular interactions. This motivated a computational study in an attempt to quantify the energy costs for these distortions. First, gas phase geometry optimizations were performed using density functional theory (DFT) at the B3LYP-6311 g(2d,p) level of theory (Figure 3). As expected,

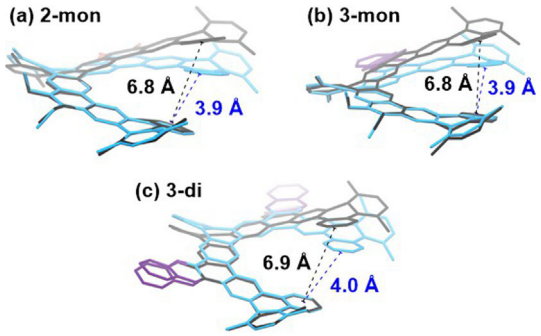

Figure 3. MicroED (black) and calculated (blue) structures of helicenes a) **2-mon**, b) **3-mon**, and c) **3-di**. The noted distances represent the pitches of the helices that are defined by the centroids of the inner 11 rings.[26]

the calculated structures display only modest pitches of 3.9 Å (**2-mon**), 3.9 Å (**3-mon**), and 4.0 Å (**3-di**), which are in much better agreement with those from previously-reported expanded helicenes (vide supra). Next, the structures were optimized with geometry constraints to approximate the pitches observed in their respective crystal structures, and the energies were compared with those from the unconstrained geometries. The energy cost for the observed molecular distortion was estimated to be 3.2, 3.2, and 3.8 kcal mol^{-1} for **2-mon**, **3-mon**, and **3-di**, respectively (see SI for details). These relatively small values provide rationale for the remarkable ability of these helicenes to "flex" in order to accommodate novel crystal packings.

Conclusion

In conclusion, the discovery of a selective oxidative dearomatization of a readily available, electron-rich expanded helicene provided access to a series of four electron deficient analogues. The five helicenes displayed variations in a range of properties, but the most notable differences were related to their solid-state structures. Despite difficulties with crystal growth and the associated failures of X-ray crystallography, the acquisition of high-resolution structural data for all helicenes was easily accomplished with MicroED. A range of unique solid-state packing behavior was observed, including four different space groups, homochirality in a crystal for a helicene with an extremely low enantiomerization barrier, nanometer scale cavities, and large molecular distortions without an obvious driving force. The latter suggests that expanded helicene flexibility may manifest in non-intuitive ways to afford unprecedented solid-state packing. Perhaps most importantly, the results of this study provide an initial indication of MicroED's potential utility for high-throughput crystallization to aid the discovery of novel organic materials.

Acknowledgements

A large portion of this work was funded by the National Science Foundation under Grant No. CHE-1708210. C.G.J.

acknowledges the National Science Foundation Graduate Research Fellowship Program (DGE-1650604), the Christopher S. Foote Fellowship, and the Pat Tillman Foundation for funding. J.O. acknowledges the National Science Foundation Graduate Research Fellowship Program (DGE-1650604) for funding. H.M.N. acknowledges the Packard Foundation and Bristol Myers Squibb for generous funding. A.E.S. thanks Robert H. Grubbs for use of facilities and helpful discussions. The authors thank Jose Rodriguez, Duilio Cascio, Michael R. Sawaya and Michael J. Collazo (UCLA) for assistance with MicroED data collection and processing, and Vincent LaVallo, Yan Xu and William Wolf for helpful general discussions. The computational work was performed at the UC Berkeley Molecular Graphics and Computation Facility (MGCF), which is supported by the National Institute of Health (Grant No. NIH S10OD023532), and the authors thank Dave Small for his assistance with these calculations. This work incorporates data collected at the Northeastern Collaborative Access Team (NE-CAT) beamlines at Argonne National Laboratory. NE-CAT is funded by the NIH-NIGMS (Grant No. P30 GM124165). The Pilatus 6M detector on the 24-ID-C beamline is funded by NIH-ORIP HEI (Grant No. S10 RR029205). This work also used resources at the Advanced Photon Source, a U.S. Department of Energy Office of Science User Facility operated by Argonne National Laboratory under Contract No. DE-AC02-06CH11357. The UCLA-DOE Institute's X-ray Crystallography Core Facility is supported by the U.S. Department of Energy (Grant No. DE-FC02-02ER63421).

Conflict of interest

The authors declare no conflict of interest.

Keywords: chiral nanocarbon · helicenes · microED · polycyclic aromatic hydrocarbon (PAH) · self-assembly

[1] a) J. R. Brandt, F. Salerno, M. J. Fuchter, *Nat. Rev. Chem.* **2017**, *1*, 0045; b) J. M. Fernández-García, P. J. Evans, S. Filippone, M. Á. Herranz, N. Martín, *Acc. Chem. Res.* **2019**, *52*, 1565 – 1574; c) M. Rickhaus, M. Mayor, M. Juríček, *Chem. Soc. Rev.* **2016**, *45*, 1542 – 1556; d) Y. Shen, C.-F. Chen, *Chem. Rev.* **2012**, *112*, 1463 – 1535; e) M. Gingras, *Chem. Soc. Rev.* **2013**, *42*, 968 – 1006; f) M. Gingras, *Chem. Soc. Rev.* **2013**, *42*, 1051 – 1095; g) K. Dhbaibi, L. Favereau, J. Crassous, *Chem. Rev.* **2019**, *119*, 8846 – 8953.

[2] a) J. E. Field, G. Muller, J. P. Riehl, D. Venkataraman, *J. Am. Chem. Soc.* **2003**, *125*, 11808 – 11809; b) Y. Yang, R. Correa da Costa, M. J. Fuchter, A. J. Campbell, *Nat. Photonics* **2013**, *7*, 634 – 638; c) H. Tanaka, Y. Inoue, T. Mori, *ChemPhotoChem* **2018**, *2*, 386 – 402.

[3] T. Verbiest, S. V. Elshocht, M. Kauranen, L. Hellemans, J. Snauwaert, C. Nuckolls, T. J. Katz, A. Persoons, *Science* **1998**, *282*, 913 – 915.

[4] V. Kiran, S. P. Mathew, S. R. Cohen, I. H. Delgado, J. Lacour, R. Naaman, *Adv. Mater.* **2016**, *28*, 1957 – 1962.

[5] a) A. R. A. Palmans, E. W. Meijer, *Angew. Chem. Int. Ed.* **2007**, *46*, 8948 – 8968; *Angew. Chem.* **2007**, *119*, 9106 – 9126; b) Y. Yang, Y. Zhang, Z. Wei, *Adv. Mater.* **2013**, *25*, 6039 – 6049; c) M. Liu, L. Zhang, T. Wang, *Chem. Rev.* **2015**, *115*, 7304 – 7397; d) E. Yashima, N. Ousaka, D. Taura, K. Shimomura, T. Ikai, K. Maeda, *Chem. Rev.* **2016**, *116*, 13752 – 13990.

[6] J. A. Schmidt, J. A. Weatherby, I. Sugden, A. Santana-Bonilla, F. Salerno, M. Fuchter, E. Johnson, J. Nelson, K. Jelfs, **2020** https://doi.org/10.26434/chemrxiv.12451943.v1.

[7] a) L. Barnett, D. M. Ho, K. K. Baldridge, R. A. Pascal, *J. Am. Chem. Soc.* **1999**, *121*, 727 – 733; b) X.-Y. Wang, X.-C. Wang, A. Narita, M. Wagner, X.-Y. Cao, X. Feng, K. Müllen, *J. Am. Chem. Soc.* **2016**, *138*, 12783 – 12786; c) T. Fujikawa, Y. Segawa, K. Itami, *J. Am. Chem. Soc.* **2015**, *137*, 7763 – 7768; d) A. Pradhan, P. Dechambenoit, H. Bock, F. Durola, *Chem. Eur. J.* **2016**, *22*, 18227 – 18235; e) Y. Hu, X.-Y. Wang, P.-X. Peng, X.-C. Wang, X.-Y. Cao, X. Feng, K. Müllen, A. Narita, *Angew. Chem. Int. Ed.* **2017**, *56*, 3374 – 3378; *Angew. Chem.* **2017**, *129*, 3423 – 3427; f) T. Hosokawa, Y. Takahashi, T. Matsushima, S. Watanabe, S. Kikkawa, I. Azumaya, A. Tsurusaki, K. Kamikawa, *J. Am. Chem. Soc.* **2017**, *139*, 18512 – 18521; g) M. Ball, Y. Zhong, Y. Wu, C. Schenck, F. Ng, M. Steigerwald, S. Xiao, C. Nuckolls, *Acc. Chem. Res.* **2015**, *48*, 267 – 276; h) C. Li, Y. Yang, Q. Miao, *Chem. Asian J.* **2018**, *13*, 884 – 894; i) N. J. Schuster, D. W. Paley, S. Jockusch, F. Ng, M. L. Steigerwald, C. Nuckolls, *Angew. Chem. Int. Ed.* **2016**, *55*, 13519 – 13523; *Angew. Chem.* **2016**, *128*, 13717 – 13721; j) P. J. Evans, J. Ouyang, L. Favereau, J. Crassous, I. Fernández, J. Perles, N. Martín, *Angew. Chem. Int. Ed.* **2018**, *57*, 6774 – 6779; *Angew. Chem.* **2018**, *130*, 6890 – 6895; k) N. J. Schuster, L. A. Joyce, D. W. Paley, F. Ng, M. L. Steigerwald, C. Nuckolls, *J. Am. Chem. Soc.* **2020**, *142*, 7066 – 7074.

[8] a) C. Nuckolls, T. J. Katz, L. Castellanos, *J. Am. Chem. Soc.* **1996**, *118*, 3767 – 3768; b) T. Hatakeyama, S. Hashimoto, T. Oba, M. Nakamura, *J. Am. Chem. Soc.* **2012**, *134*, 19600 – 19603; c) Y. Yang, B. Rice, X. Shi, J. R. Brandt, R. Correa da Costa, G. J. Hedley, D.-M. Smilgies, J. M. Frost, I. D. W. Samuel, A. Otero-de-la-Roza, E. R. Johnson, K. E. Jelfs, J. Nelson, A. J. Campbell, M. J. Fuchter, *ACS Nano* **2017**, *11*, 8329 – 8338; d) P. Josse, L. Favereau, C. Shen, S. Dabos-Seignon, P. Blanchard, C. Cabanetos, J. Crassous, *Chem. Eur. J.* **2017**, *23*, 6277 – 6281; e) M. A. Shcherbina, X. Zeng, T. Tadjiev, G. Ungar, S. H. Eichhorn, K. E. S. Phillips, T. J. Katz, *Angew. Chem. Int. Ed.* **2009**, *48*, 7837 – 7840; *Angew. Chem.* **2009**, *121*, 7977 – 7980.

[9] a) G. R. Kiel, S. C. Patel, P. W. Smith, D. S. Levine, T. D. Tilley, *J. Am. Chem. Soc.* **2017**, *139*, 18456 – 18459; b) Y. Nakakuki, T. Hirose, K. Matsuda, *J. Am. Chem. Soc.* **2018**, *140*, 15461 – 15469; c) G. R. Kiel, K. L. Bay, A. E. Samkian, N. J. Schuster, J. B. Lin, R. C. Handford, C. Nuckolls, K. N. Houk, T. D. Tilley, *J. Am. Chem. Soc.* **2020**, *142*, 11084 – 11091; d) K. Fujise, E. Tsurumaki, G. Fukuhara, N. Hara, Y. Imai, S. Toyota, *Chem. Asian J.* **2020**, *15*, 2456 – 2461.

[10] a) C. G. Jones, M. W. Martynowycz, J. Hattne, T. J. Fulton, B. M. Stoltz, J. A. Rodriguez, H. M. Nelson, T. Gonen, *ACS Cent. Sci.* **2018**, *4*, 1587 – 1592; b) C. G. Jones, M. Asay, L. J. Kim, J. F. Kleinsasser, A. Saha, T. J. Fulton, K. R. Berkley, D. Cascio, A. G. Malyutin, M. P. Conley, B. M. Stoltz, V. Lavallo, J. A. Rodríguez, H. M. Nelson, *ACS Cent. Sci.* **2019**, *5*, 1507 – 1513; c) B. L. Nannenga, *Struct. Dyn.* **2020**, *7*, 014304; d) A. M. Levine, G. Bu, S. Biswas, E. H. R. Tsai, A. B. Braunschweig, B. L. Nannenga, *Chem. Commun.* **2020**, *56*, 4204 – 4207.

[11] Z. Chen, A. Lohr, C. R. Saha-Möller, F. Würthner, *Chem. Soc. Rev.* **2009**, *38*, 564 – 584.

[12] a) C. A. Liberko, L. L. Miller, T. J. Katz, L. Liu, *J. Am. Chem. Soc.* **1993**, *115*, 2478 – 2482; b) D. Schweinfurth, M. Zalibera, M. Kathan, C. Shen, M. Mazzolini, N. Trapp, J. Crassous, G. Gescheidt, F. Diederich, *J. Am. Chem. Soc.* **2014**, *136*, 13045 – 13052; c) D. Schweinfurth, M. Mazzolini, D. Neshchadin, C. Hoyer, R. Geier, K. Gatterer, N. Trapp, G. Gescheidt, F. Diederich, *Chem. Eur. J.* **2016**, *22*, 7152 – 7157.

[13] a) R. A. Pascal, W. D. McMillan, D. Van Engen, R. G. Eason, *J. Am. Chem. Soc.* **1987**, *109*, 4660 – 4665; b) Z. Wang, Ž. Tomović,

M. Kastler, R. Pretsch, F. Negri, V. Enkelmann, K. Müllen, *J. Am. Chem. Soc.* **2004**, *126*, 7794 – 7795; c) D. Wasserfallen, M. Kastler, W. Pisula, W. A. Hofer, Y. Fogel, Z. Wang, K. Müllen, *J. Am. Chem. Soc.* **2006**, *128*, 1334 – 1339.

[14] Z. Wang, P. Lu, S. Chen, Z. Gao, F. Shen, W. Zhang, Y. Xu, H. S. Kwok, Y. Ma, *J. Mater. Chem.* **2011**, *21*, 5451 – 5456.

[15] a) Y. Fogel, M. Kastler, Z. Wang, D. Andrienko, G. J. Bodwell, K. Müllen, *J. Am. Chem. Soc.* **2007**, *129*, 11743 – 11749; b) U. H. F. Bunz, J. U. Engelhart, B. D. Lindner, M. Schaffroth, *Angew. Chem. Int. Ed.* **2013**, *52*, 3810 – 3821; *Angew. Chem.* **2013**, *125*, 3898 – 3910; c) A. Mateo-Alonso, *Chem. Soc. Rev.* **2014**, *43*, 6311 – 6324.

[16] a) H. Sakai, S. Shinto, Y. Araki, T. Wada, T. Sakanoue, T. Takenobu, T. Hasobe, *Chem. Eur. J.* **2014**, *20*, 10099 – 10109; b) Y. Sun, X. Li, C. Sun, H. Shen, X. Hou, D. Lin, H.-L. Zhang, C. Di, D. Zhu, X. Shao, *Angew. Chem. Int. Ed.* **2017**, *56*, 13470 – 13474; *Angew. Chem.* **2017**, *129*, 13655 – 13659.

[17] a) B. N. Boden, K. J. Jardine, A. C. W. Leung, M. J. MacLachlan, *Org. Lett.* **2006**, *8*, 1855 – 1858; b) R. Rieger, M. Kastler, V. Enkelmann, K. Müllen, *Chem. Eur. J.* **2008**, *14*, 6322 – 6325.

[18] "Forty Years of Clar's Aromatic π-Sextet Rule": M. Solà, *Front. Chem.* **2013**, https://doi.org/10.3389/fchem.2013.00022.

[19] E. J. Moriconi, B. Rakoczy, W. F. O'Connor, *J. Org. Chem.* **1962**, *27*, 2772 – 2776.

[20] D. M. Togashi, D. E. Nicodem, *Spectrochim. Acta Part A* **2004**, *60*, 3205 – 3212.

[21] CV data was also acquired in THF solution (Figure S21), which is a better solvent for probing reduction events. For example, **2-mon** exhibits two reversible waves in THF versus only one in CH_2Cl_2.

[22] Due to the dynamic nature of the self-assembling system, the measurements do not yield accurate information on specific aggregate size, but rather function as a tool for qualitative comparisons. See also: W. Wang, J. J. Han, L.-Q. Wang, L.-S. Li, W. J. Shaw, A. D. Q. Li, *Nano Lett.* **2003**, *3*, 455 – 458.

[23] a) A. S. Shetty, J. Zhang, J. S. Moore, *J. Am. Chem. Soc.* **1996**, *118*, 1019 – 1027; b) I. Horman, B. Dreux, *Helv. Chim. Acta* **1984**, *67*, 754 – 764.

[24] In general, crystals were 10–50 μm by 1–2 μm needles or rods.

[25] a) S. Øien-Ødegaard, G. C. Shearer, D. S. Wragg, K. P. Lillerud, *Chem. Soc. Rev.* **2017**, *46*, 4867 – 4876; b) C. X. Weichenberger, P. V. Afonine, K. Kantardjieff, B. Rupp, *Acta Crystallogr. Sect. D* **2015**, *71*, 1023 – 1038.

[26] Pitches were calculated by fitting a helical curve to the 11 centroids of the inner rings, using the HELFIT program developed by Enkhbayar and co-workers (see SI for details): P. Enkhbayar, S. Damdinsuren, M. Osaki, N. Matsushima, *Comput. Biol. Chem.* **2008**, *32*, 307 – 310.

Manuscript received: September 7, 2020
Accepted manuscript online: October 8, 2020
Version of record online: ■■ ■■, ■■■■

Research Articles

Helicenes

A. E. Samkian, G. R. Kiel, C. G. Jones, H. M. Bergman, J. Oktawiec, H. M. Nelson,* T. D. Tilley* _____ ▮▮▮▮–▮▮▮▮

Elucidation of Diverse Solid-State Packing in a Family of Electron-Deficient Expanded Helicenes via Microcrystal Electron Diffraction (MicroED)

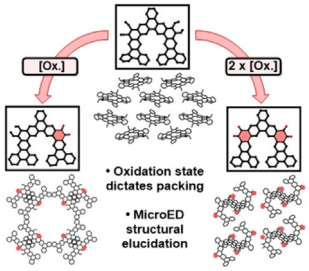

A set of five diverse expanded helicenes was accessed through divergent functionalization and characterized using microcrystal electron diffraction (MicroED), revealing previously inaccessible structural data. Features such as long range π-stacking, homochiral crystals, and emergent nanometer scale cavities were observed, spanning four different space groups.